Available online at www.sciencedirect.com

SciVerse ScienceDirect

Ceramics International 39 (2013) 3685–3689

CERAMICS INTERNATIONAL

www.elsevier.com/locate/ceramint

Visible-light sensitive $La_{1-x}Ba_xCoO_3$ photocatalyst for malachite green degradation

Chunqiu Zhang, Hongcai He*, Ning Wang, Haijun Chen, Deting Kong

State Key Laboratory of Electronic Thin Films and Integrated Devices and School of Microelectronics and Solid-State Electronics, University of Electronic Science and Technology of China, Chengdu 610054, PR China

Received 18 September 2012; received in revised form 11 October 2012; accepted 12 October 2012
Available online 22 October 2012

Abstract

In this study, a series of photocatalyst $La_{1-x}Ba_xCoO_3$ ($x=0$, 0.1, 0.3, 0.5, 0.7) powders were successfully prepared using the sol–gel method. The crystal structure and band gap of $La_{1-x}Ba_xCoO_3$ were characterized by X-ray diffraction and Ultraviolet–visible diffuse reflection spectroscopy for photocatalysis investigation. The results showed that the Ba-doped $LaCoO_3$ exhibited obvious absorption characteristics in visible light regions. In addition, the effect of $La_{1-x}Ba_xCoO_3$ on the photocatalytic degradation of malachite green under different light sources was also investigated. Ba-doped $LaCoO_3$ showed excellent visible-light sensitive photocatalytic activities and a maximum photocatalytic degradation of malachite green could be achieved with a degradation degree of 97% by $La_{0.7}Ba_{0.3}CoO_3$ in visible light for 60 min.

Keywords: Ba-doped $LaCoO_3$; Photocatalysis; Degradation; Malachite green

1. Introduction

Pollutant degradation has gained considerable attention because of increasing environmental pollution. Since Fujishima and Honda reported the photocatalytic splitting of water into oxygen and hydrogen using TiO_2 in 1972 [1], environment-friendly photocatalysis using solar energy has become a promising approach in solving pollutant degradation problems. In the past decades, numerous valuable and interesting studies on the preparation of photocatalytic materials have been investigated [2], thereby developing new kinds of photocatalysts. Among these photocatalysts, much attention has been paid to oxide photocatalysts, such as TiO_2 [3,4], ZnO [5], and Fe_2O_3 [6], because of their simplicity, low-cost, and environment friendliness. However, several simple oxides, including TiO_2, absorb only ultraviolet light when initiating photocatalytic reaction because of their wide band gaps [7,8]. This characteristic limits the photocatalysis application of simple oxides because ultraviolet light accounts for only 7%–8% of the total sunlight. Therefore, researchers have focused on photocatalysts that are sensitive to visible light [7] and near infrared light [9]. Several effective studies have been conducted for the modification of simple oxides to generate donor or acceptor states in the band gap by adding controlled metal [10] or nonmetal impurities [11]. Chen et al. [12] demonstrated a new approach in enhancing solar absorption by introducing disorders in the surface layers of nanophase TiO_2 through hydrogenation.

Various new oxide photocatalysts have been investigated. A number of multiple complex oxides, such as $SrTiO_3$ [13], $BiVO_4$ [14,15], $LaCoO_3$ [16], and Bi_2WO_6 [17], have been demonstrated as promising photocatalysts because of their strong visible light absorption and high quantum efficiency. These multiple complex oxides have better photocatalytic activity than TiO_2 under sunlight [18]. Further research indicated that the photocatalysis of perovskite-based materials can be improved by doping [19–21]. For example, cobalt-doped $BiVO_4$ [14] exhibits greater photocatalytic activity than pure $BiVO_4$ in methylene blue decolorization. In addition, C-doped $LaCoO_3$ photocatalysts [16] have higher photocatalytic activities under visible light than un-doped $LaCoO_3$ in carbon

*Corresponding author. Tel.: +86 28 83203807; fax: +86 28 832 02569.
E-mail address: hehc@uestc.edu.cn (H. He).

0272-8842/$ - see front matter © 2012 Elsevier Ltd and Techna Group S.r.l. All rights reserved.
http://dx.doi.org/10.1016/j.ceramint.2012.10.200

dioxide reduction. To date, the magnetic property, gas-sensitivity, and potential double-perovskite structure of Ba-doped $LaCoO_3$ have drawn considerable attention [22]. Excellent mixed ionic–electronic conductivity, with fast surface exchange coefficients in double perovskite cobaltates and oxygen defects due to different ion valence states and ion radii between Ba^{2+} and La^{3+}, affects the photocatalytic activity of Ba^{2+} and La^{3+}. Little attention, however, has been paid on this topic.

In this study, perovskite $La_{1-x}Ba_xCoO_3$ nano-powder photocatalysts were synthesized through the sol–gel method. The crystal structures and photoabsorption characteristics of the nano powders were studied to investigate the Ba-doping effect. Moreover, the photocatalytic activity of $La_{1-x}Ba_xCoO_3$ nano powders for the photodegradation of organic dye malachite green was investigated.

2. Experimental

$La_{1-x}Ba_xCoO_3$ ($x=0$, 0.1, 0.3, 0.5, 0.7) nano-powders were prepared from citrate precursors via the sol–gel method, as reported by Predoana et al. [23]. $La(NO_3)_3\cdot 6H_2O$, $Ba(NO_3)_2$, and $Co(NO_3)_2\cdot 6H_2O$ were dissolved in deionized water according to the stoichiometric ratio to obtain a specific concentrated solution. Excess citric acid was added to the solution as chelating agent. Appropriate amounts of polyethylene glycol 400 were then added into the mixture as dispersion agent. The mixture was continually stirred at 80 °C after ultrasonic mixing until a transparent solution was achieved. The products were dried at 110 °C and presintered at 40 °C for 2 h. The nano-powders were obtained by grinding the presintered products and calcining at 750 °C for 2 h.

X-ray diffraction (XRD; Rigaku D/MAX-RB, Japan) with CuKa radiation was used for the phase analysis of the powders under 40 kV and 30 mA. Scanning electron microscopy (SEM; INSPECTF FEI, Netherlands) was used to observe the microstructures. Ultraviolet–visible (UV–vis) diffuse reflection spectroscopy of the photocatalyst was investigated with a U-3010 Hitachi UV–vis spectrophotometer using $BaSO_4$ as reference.

Photocatalytic reaction was carried out in a beaker containing a magnetic stirrer. The reaction suspension was prepared by adding certain amounts of photocatalysts into a 30 mL aqueous malachite green solution at 10 mg/L. The mixture was ultrasonically dispersed for 30 min in the dark to reach the adsorption–desorption equilibrium. Subsequently, the mixture was continually stirred for 60 min under Xenon Light, with an UV cutoff filter ($\lambda > 420$ nm) as visible light, and a commercial 250 W high-pressure Hg lamp, with a maximum emission wavelength of 365 nm. Samples were taken at regular intervals from the mixture and centrifuged to remove the particles for measurement. The degradation degree of malachite green was determined using a UV–vis spectrophotometer (Beijing Puxi) according to the following equation: $D\% = (c_0 - c)/c_0 \times 100\% = (A_0 - A)/A_0 \times 100\%$, where c_0 and c are the initial concentration and concentration after photocatalysis of the solution, respectively; and A_0 and A are the absorption intensities before and after photocatalytic reaction, respectively.

3. Results and discussions

The XRD patterns of the $La_{1-x}Ba_xCoO_3$ ($x=0$, 0.1, 0.3, 0.5, 0.7) phocatalysts are shown in Fig. 1. The patterns indicate that $La_{1-x}Ba_xCoO_3$ ($x=0$, 0.1, 0.3, 0.5) maintains a perovskite structure similar to $LaCoO_3$ without any impurity phases. On the contrary, some impurity phases such as $BaCoO_2$ and BaO_2 were observed in the $La_{0.3}Ba_{0.7}CoO_3$ ($x=0.7$) pattern. In other words, Ba atoms can enter the crystal lattice and replace the La atoms to occupy A site in the $LaCoO_3$ crystal structure for $La_{0.3}Ba_{0.7}CoO_3$; however, large quantities of Ba ($x=0.7$) produce impurity phase. The patterns also show that the double peaks at $2\theta = 32°$, 59°, and 69° change to single peaks as the Ba substitution increases from 0 to 0.5. $La_{1-x}Ba_xCoO_3$ ($x=0$, 0.1, 0.3) have rhombohedral structures (space group R3c) that refer to standard diffraction data (JCPDS 48-0123) [24], whereas $La_{0.5}Ba_{0.5}CoO_3$ has a cubic crystal structure [25]. The difference in crystal structures results in the transformation of double peaks to single peaks. The diffraction peaks shift toward a lower 2θ value with increasing Ba(x) fraction because of the larger ionic radius of Ba than that of La. This shift also indirectly demonstrates that Ba atoms replace La atoms and affect the crystal lattice. Therefore, the cell parameters of rhombohedral $La_{1-x}Ba_xCoO_3$ ($x=0$, 0.1, 0.3) are 5.435, 5.448, and 5.469, respectively. The XRD patterns show that the cell parameter of the cubic $La_{0.5}Ba_{0.5}CoO_3$ is 5.491. SEM studies were performed to verify the morphology and particle size of the photocatalysts (Fig. 2). Fig. 2 shows the SEM image of the $La_{0.7}Ba_{0.3}CoO_3$ powders, with a uniform particle size of approximately 70 nm–80 nm. No obvious variations were observed with the changes in the $La_{1-x}Ba_xCoO_3$ composition.

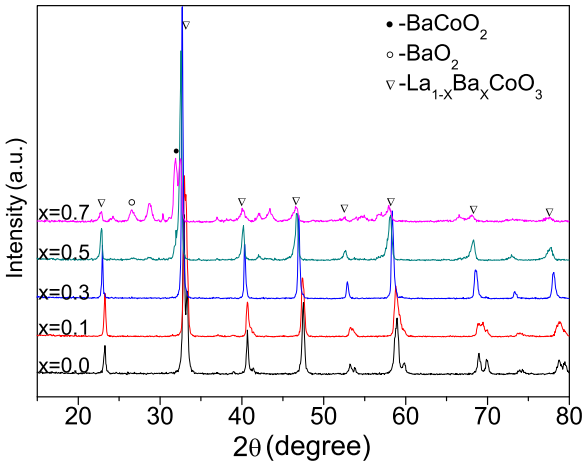

Fig. 1. XRD patterns of $La_{1-x}Ba_xCoO_3$ ($x=0$, 0.1, 0.3, 0.5, 0.7) nano powders.

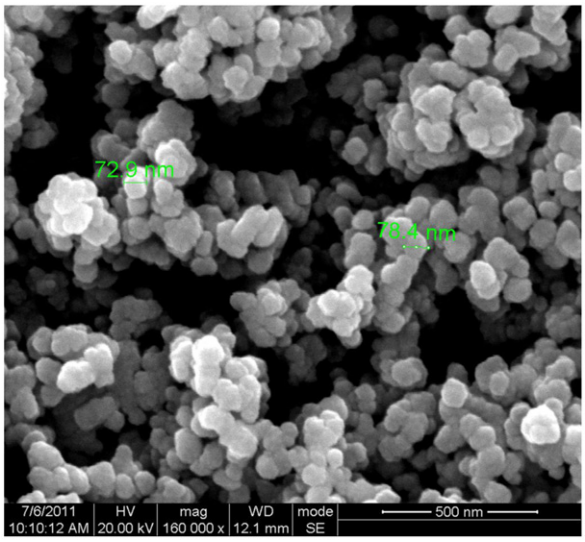

Fig. 2. SEM image of $La_{1-x}Ba_xCoO_3$ (x=0.3) nano powders.

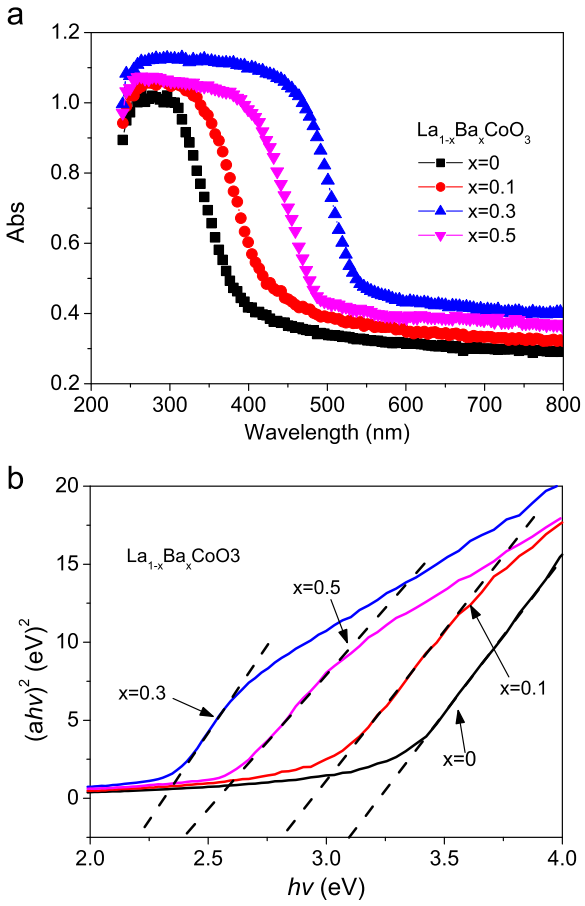

Fig. 3. UV–vis diffuse absorption spectra (a) and estimated band gap (b) of $La_{1-x}Ba_xCoO_3$ photocatalysts.

The diffuse reflectance spectra of the photocatalysts are shown in Fig. 3a. Doping $LaCoO_3$ with Ba increases light absorption in the UV and visible light regions. Particularly, $La_{0.7}Ba_{0.3}CoO_3$ exhibits strong absorption of visible light with wavelengths shorter than 540 nm. The band-gap values for the photocatalysts were obtained by the Kubelka-Munk function from the patterns in the UV–vis region of the samples. Specifically, the band gap values were determined by the interception of the straight line fitted through the low-energy side of the curve $[F(R)\cdot h\upsilon]^2$ versus $h\upsilon$, where $F(R)$ is the Kubelka-Munk function and $h\upsilon$ is the energy of the incident photon [16,26]. Fig. 3b shows that the band gap of $LaCoO_3$ is 3.09 eV according to the optical absorption thresholds at 401 nm. The band gap of $La_{1-x}Ba_xCoO_3$ (x=0.1, 0.3, 0.5) are 2.80 eV, 2.21 eV, and 2.40 eV according to the optical absorption thresholds at 443 nm, 561 nm, and 516 nm, respectively. Ba-doped $LaCoO_3$ shows better absorption in the visible light region and lower band-gap than pure $LaCoO_3$. Band gap decreases with increasing Ba substitution. However, $La_{0.5}Ba_{0.5}CoO_3$ reveals a higher band gap than $La_{0.7}Ba_{0.3}CoO_3$. The high band gap is caused by the cubic crystal structure of $La_{0.5}Ba_{0.5}CoO_3$, which differs from the rhombohedral structures of $La_{1-x}Ba_xCoO_3$ (x=0, 0.1, 0.3).

The degradation of aqueous malachite green solution was performed under UV and visible-light irradiation to explore the photocatalytic activity of the $La_{1-x}Ba_xCoO_3$ samples. The results are shown in Fig. 4. The degradation efficiency of malachite green significantly increases with

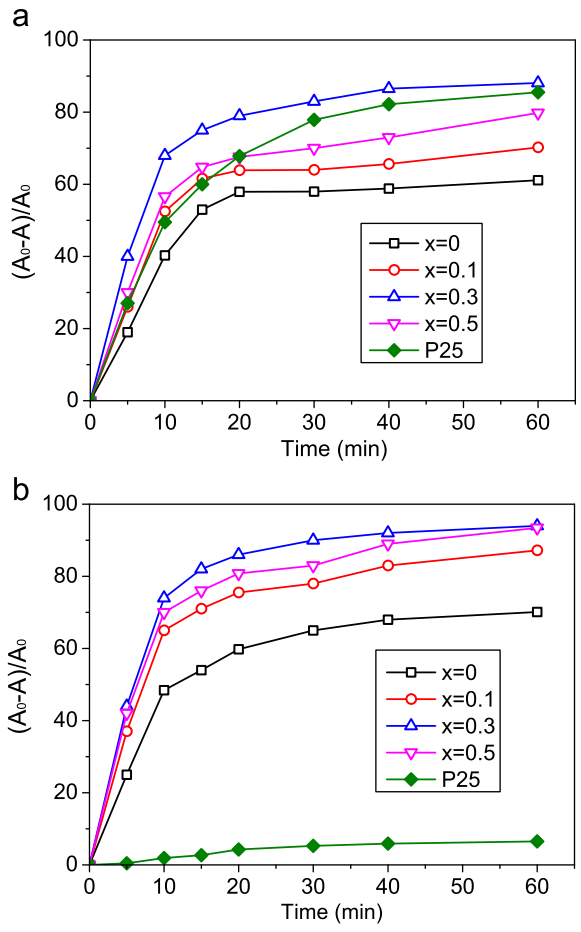

Fig. 4. Photocatalytic degradation of malachite green with $La_{1-x}Ba_xCoO_3$ (x=0, 0.1, 0.3, 0.5) catalysts under: (a) UV light and (b) visible light.

increasing time, and then equilibrates after 30 min of photocatalytic reaction under either UV light or visible light. After 60 min of irradiation under UV light, malachite green degradation by $La_{1-x}Ba_xCoO_3$ (x=0, 0.1, 0.3, 0.5) reached 59.7%, 70.2%, 88.1%, and 79.8%, respectively (Fig. 4a). After 60 min under visible light, the degradation of malachite green by $La_{1-x}Ba_xCoO_3$ (x=0, 0.1, 0.3, 0.5) reached 70.1%, 87.2%, 97.0%, and 93.4%, respectively (Fig. 4b), greatly higher than those under UV light. This result indicates that Ba-doped $LaCoO_3$ exhibits better photocatalytic activity for the degradation of malachite green under visible light than under UV light. In both cases, all Ba-doped samples exhibited slightly higher activity than pure $LaCoO_3$. The photocatalytic degradation performance increases with the increase of Ba stoichiometry x to 0.3; however, the degradation efficiency decreases when Ba stoichiometry x further increases to 0.5. In other words, $La_{0.7}Ba_{0.3}CoO_3$ exhibits the best degradation efficiency because of its smallest band gap. For comparison, the photocatalytic degradation performance of a typical commercial TiO_2 (P25) was measured under the same condition as the reference, which has good photocatalytic activity under UV light. Fig. 4a shows that $La_{1-x}Ba_xCoO_3$ exhibits a comparable photocatalytic degradation performance under UV light as that of P25. Under visible light, P25 exhibits poor photocatalytic activities in the photodegradation of malachite green, whereas $La_{1-x}Ba_xCoO_3$ still maintains good performance (Fig. 4b).

Semiconductor photocatalysts can absorb radiation with energies equal to or greater than its band-gap energy. Semiconductor photocatalysts can also induce charge carriers that can react directly with absorbed organics, water, oxygen, or –OH on the catalyst to produce $\cdot OH$ and $O_2^{\cdot}$ with high oxidization activities. For $La_{1-x}Ba_xCoO_3$, substitutions of La^{3+} by Ba^{2+} can induce excess negative charges in the lattice, which must be compensated by positive charges according to the electroneutrality principle. Consequently, Co^{3+} oxidizes to Co^{4+} or creates oxygen vacancies to maintain electroneutrality conditions [27,28]. The absorption quantity of oxygen on the photocatalyst surface increases with the addition of oxygen vacancies, resulting in the enhancement of carrier-induced and oxygen-absorbed reaction centers, thereby, improving the photocatalysis of $La_{1-x}Ba_xCoO_3$ (x=0.1, 0.3, 0.5). In addition, Ba-doping can produce defect levels in the interspace of conduction band and valence band. The defect levels function as "steps" that aid electron transit, corresponding to the narrow band-gap identical to the result in Fig. 2. Therefore, the photocatalysis activity and absorption range in the visible light region is increased after doping.

During photocatalytic treatment, the input amount of the photocatalysts is an important factor related with costs and optimum results. The concentration effect of the photocatalysts was investigated on the degradation of similar amounts of malachite green solution under visible light. The photocatalysts $La_{0.7}Ba_{0.3}CoO_3$, which are optimal for the degradation of malachite green, was added to 30 mL malachite green solution (10 mg/L) to achieve different concentrations of $La_{0.7}Ba_{0.3}CoO_3$ from 0.1 g/L to 10 g/L. The photocatalytic degradation efficiency after 60 min of irradiation under visible light is shown in Fig. 5.

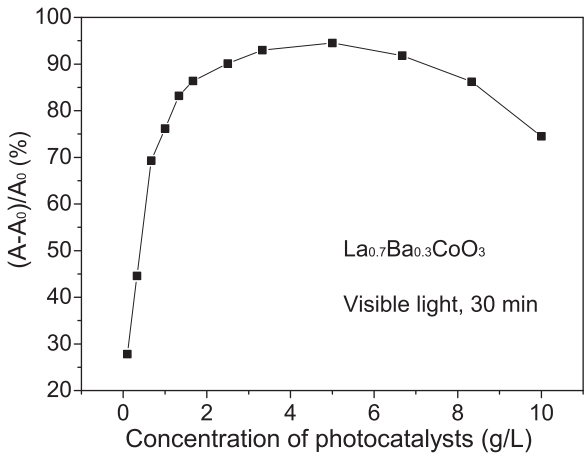

Fig. 5. Photocatalytic degradation of malachite green with different concentrations of $La_{0.7}Ba_{0.3}CoO_3$.

The degradation performance of malachite green increases with increasing concentrations of $La_{0.7}Ba_{0.3}CoO_3$ and reaches the maximum degradation efficiency of 94.5% at 5 g/L. However, increasing the concentration from 5 g/L to 10 g/L decreases the degradation effect. The total specific surface area of the photocatalysts in the container was investigated to explain the variations in degradation efficiency [17], which dominated the adsorption capacity of the malachite green dye participating in photocatalytic reactions. Elevated photocatalysts concentrations enlarged the total specific surface area of the photocatalyst nanopowder and provided increased amounts of photocatalytic reaction centers, thereby, increasing photocatalytic degradation efficiency. Nevertheless, when the solution reaches a certain concentration, (e.g., 5 g/L for $La_{0.7}Ba_{0.3}CoO_3$ with the current situation) nanoparticles are aggregated and their specific surface area decreased. Thus, increasing the photocatalyst concentrations weaken the photocatalytic degradation efficiency because of the nanoparticle aggregation.

4. Conclusions

In summary, Ba-doped $LaCoO_3$ photocatalysts with different Ba contents were successfully synthesized using the sol–gel method. The photocatalysts have uniform particle sizes of approximately 70 nm–80 nm without any impurity phases. Ba doping narrowed the band gap, as estimated by UV–vis diffuse reflectance spectroscopy, and resulted in higher visible-light sensitive photocatalytic activities compared with un-doped photocatalysts. The replacement of La^{3+} with Ba^{2+} resulted in the coexistence of Co^{3+} and Co^{4+} and increased oxygen vacancies.

Obvious degradation of malachite green was observed with the $La_{1-x}Ba_xCoO_3$ photocatalyst under UV and visible light irradiation. Moreover, $La_{0.7}Ba_{0.3}CoO_3$ showed optimal photocatalytic degradation with a degradation degree of 97% in the visible light for 60 min.

Acknowledgment

This work was supported by the Natural Science Foundation of China (51002020, 51272035 and 51272037), the International Cooperation MOST-JST Program Fund (no. 2010DFA61410), The Project of International Cooperation of the Ministry of Science and Technology of China (no. 2011DFA50530) and the Sichuan International Science & Technology Cooperation and Communication Research Program (no. 2011HH0002).

References

[1] A. Fujishima, K. Honda, Electrochemical photolysis of water at a semiconductor electrode, Nature 238 (1972) 37–38.
[2] D.S. Bhatkhande, V.G. Pangarkar, A.A.C.M. Beenackers, Photocatalytic degradation for environmental applications—a review, Journal of Chemical Technology and Biotechnology 77 (2002) 102–116.
[3] C. Suwanchawalit, S. Wongnawa, P. Sriprang, P. Meanha, Enhancement of the photocatalytic performance of Ag-modified TiO_2 photocatalyst under visible light, Ceramics International 38 (2012) 5201–5207.
[4] M.-C. Wang, H.-J. Lin, C.-H. Wang, H.-C. Wu, Effects of annealing temperature on the photocatalytic activity of N-doped TiO_2 thin films, Ceramics International 38 (2012) 195–200.
[5] S. Suwanboon, P. Amornpitoksuk, N. Muensit, Dependence of photocatalytic activity on structural and optical properties of nanocrystalline ZnO powders, Ceramics International 37 (2011) 2247–2253.
[6] C.X. Kronawitter, S.S. Mao, B.R. Antoun, Doped, porous iron oxide films and their optical functions and anodic photocurrents for solar water splitting, Applied Physics Letters 98 (2011) 092108.
[7] H. Kisch, W. Macyk, Visible-light photocatalysis by modified titania, Chemphyschem 3 (2002) 399–400.
[8] W. Asghar, I.A. Qazi, H. Ilyas, A.A. Khan, M.A. Awan, M.R. Aslam, Comparative solid phase photocatalytic degradation of polythene films with doped and undoped TiO_2 nanoparticles, Journal of Nanomaterials 2011 (2011) 461930.
[9] C. Li, F. Wang, J. Zhu, J.C. Yu, $NaYF_4$:Yb,Tm/CdS composite as a novel near-infrared-driven photocatalyst, Applied Catalysis B-Environmental 100 (2010) 433–439.
[10] W.Y. Choi, A. Termin, M.R. Hoffmann, The role of metal-ion dopants in quantum-sized TiO_2: correlation between photoreactivity and charge-carrier recombination dynamics, Journal of Physical Chemistry 98 (1994) 13669–13679.
[11] R. Asahi, T. Morikawa, T. Ohwaki, K. Aoki, Y. Taga, Visible-light photocatalysis in nitrogen-doped titanium oxides, Science 293 (2001) 269–271.
[12] X.B. Chen, L. Liu, P.Y. Yu, S.S. Mao, Increasing solar absorption for photocatalysis with black hydrogenated titanium dioxide nanocrystals, Science 331 (2011) 746–750.
[13] N. Wang, D. Kong, H. He, Solvothermal synthesis of strontium titanate nanocrystallines from metatitanic acid and photocatalytic activities, Powder Technology 207 (2011) 470–473.
[14] B. Zhou, X. Zhao, H. Liu, J. Qu, C.P. Huang, Visible-light sensitive cobalt-doped $BiVO_4$ (Co–$BiVO_4$) photocatalytic composites for the degradation of methylene blue dye in dilute aqueous solutions, Applied Catalysis B-Environmental 99 (2010) 214–221.
[15] Y. Wan, S. Wang, W. Luo, L. Zhao, Impact of preparative pH on the morphology and photocatalytic activity of $BiVO_4$, International Journal of Photoenergy 2012 (2012) 392865.
[16] L.S. Jia, J.J. Li, W.P. Fang, H. Song, Q.B. Li, Y. Tang, Visible-light-induced photocatalyst based on C-doped $LaCoO_3$ synthesized by novel microorganism chelate method, Catalysis Communications 10 (2009) 1230–1234.
[17] Y.J. Chen, Y.Q. Zhang, C. Liu, A.M. Lu, W.H. Zhang, Photodegradation of malachite green by nanostructured Bi_2WO_6 visible light-induced photocatalyst, International Journal of Photoenergy 2012 (2012) 510158.
[18] Z.G. Zou, H. Arakawa, Direct water splitting into H_2 and O_2 under visible light irradiation with a new series of mixed oxide semiconductor photocatalysts, Journal of Photochemistry and Photobiology A 158 (2003) 145–162.
[19] D.W. Hwang, H.G. Kim, J.S. Lee, J. Kim, W. Li, S.H. Oh, Photocatalytic hydrogen production from water over M-doped $La_2Ti_2O_7$ (M=Cr, Fe) under visible light irradiation ($\lambda > 420$ nm), Journal of Physical Chemistry B 109 (2004) 2093–2102.
[20] N. Li, A. Boréave, J.-P. Deloume, F. Gaillard, Catalytic combustion of toluene over a Sr and Fe substituted $LaCoO_3$ perovskite, Solid State Ionics 179 (2008) 1396–1400.
[21] D. Wang, T. Kako, J. Ye, Efficient photocatalytic decomposition of acetaldehyde over a solid-solution perovskite $(Ag_{0.75}Sr_{0.25})(Nb_{0.75}Ti_{0.25})O_3$ under visible-light irradiation, Journal of the American Chemical Society 130 (2008) 2724–2725.
[22] J. Liu, G. Collins, M. Liu, C.L. Chen, J. Jiang, E.I. Meletis, Q. Zhang, C. Dong, PO_2 dependant resistance switch effect in highly epitaxial (LaBa)$Co_2O_{5+\delta}$ thin films, Applied Physics Letters 97 (2010) 094101.
[23] L. Predoana, B. Malic, M. Kosec, M. Carata, M. Caldararu, M. Zaharescu, Characterization of $LaCoO_3$ powders obtained by water-based sol–gel method with citric acid, Journal of the European Ceramic Society 27 (2007) 4407–4411.
[24] O. Haas, R.P.W.J. Struis, J.M. McBreen, Synchrotron X-ray absorption of $LaCoO_3$ perovskite, Journal of Solid State Chemistry 177 (2004) 1000–1010.
[25] A. Mineshige, M. Inaba, T. Yao, Z. Ogumi, K. Kikuchi, M. Kawase, Crystal structure and metal–insulator transition of $La_{1-x}Sr_xCoO_3$, Journal of Solid State Chemistry 121 (1996) 423–429.
[26] R.S.G. Ferreira, P.G.P. de Oliveira, F.B. Noronha, The effect of the nature of vanadium species on benzene total oxidation, Applied Catalysis B-Environmental 29 (2001) 275–283.
[27] D. Ferri, L. Forni, Methane combustion on some perovskite-like mixed oxides, Applied Catalysis B-Environmental 16 (1998) 119–126.
[28] A. Mineshige, M. Kobune, S. Fujii, Z. Ogumi, M. Inaba, T. Yao, K. Kikuchi, Metal-insulator transition and crystal structure of $La_{1-x}Sr_xCoO_3$ as functions of Sr-content, temperature, and oxygen partial pressure, Journal Of Solid State Chemistry 142 (1999) 374–381.